Measurements, Theory, and Modeling of OH Formation in Ethyl + O_2 and Propyl + O_2 Reactions

John D. DeSain, Stephen J. Klippenstein, James A. Miller, and Craig A. Taatjes*

Combustion Research Facility, Mail Stop 9055, Sandia National Laboratories, Livermore, California 94551-0969

Received: October 7, 2002; In Final Form: March 6, 2003

The time-resolved formation of OH from ethyl + O_2 and propyl + O_2 reactions has been measured by OH laser-induced fluorescence in pulsed-photolytic Cl-initiated oxidation of ethane and propane between 296 and 700 K. The propane oxidation produces more OH at each temperature than does ethane oxidation. Above 600 K, the peak amplitudes of the OH signals from both reactions increase sharply with increasing temperature. Solutions to the time-dependent master equation for the $C_2H_5 + O_2$, *i*-$C_3H_7 + O_2$, and *n*-$C_3H_7 + O_2$ reactions, employing previously published ab initio characterizations of the stationary points of the systems, have been used to produce temperature-dependent parameterizations that predict the rate constants for formation of all of the products (R + O_2, RO_2, QOOH, OH + aldehydes, OH + O-heterocycles, HO_2 + alkene). These parameterizations are utilized in rate equation models to compare to experimental results for HO_2 and OH formation in Cl-initiated ethane and propane oxidation. The models accurately describe the time behavior and amplitude of the HO_2 from both oxidation systems. However, the model underpredicts the amount of OH observed at high temperatures (>600 K) and overpredicts the amount of OH observed at lower temperatures (≤600 K).

Introduction

The reactions of alkyl radicals, R, with molecular oxygen are central to atmospheric hydrocarbon oxidation and to low temperature combustion phenomena such as autoignition and engine knock. Correspondingly, they have been the subject of a large number of experimental and theoretical studies, and a very detailed understanding of their mechanism has evolved. The initial step generally involves the formation of an alkylperoxy complex, RO_2

$$R + O_2 \leftrightarrow RO_2 \quad (1a)$$

Gutman, Slagle, Knyazev, and co-workers[1−5] have measured equilibrium constants for this initial addition for many alkyl and substituted alkyl radicals. Direct elimination from RO_2 is now known to be the principal mechanism for alkene + HO_2 formation

$$RO_2 \rightarrow \text{alkene} + HO_2 \quad (1b)$$

Alternatively, the RO_2 radical can isomerize via intramolecular hydrogen transfers to form a variety of different hydroperoxyalkyl radicals, usually denoted QOOH

$$RO_2 \leftrightarrow QOOH \quad (1c)$$

Decomposition of the QOOH species via OO bond fission appears to provide the primary route to forming OH

$$QOOH \leftrightarrow \text{O-heterocycle} + OH \quad (1d)$$

The branching between OH and HO_2 affects chain propagation, and reactions of QOOH with O_2 are thought to be responsible for chain branching in low temperature (∼600−800 K) oxidation. A QOOH species is also the antecedent to product channel 1d and our understanding of the isomerization process is largely due to investigations by Walker and coworkers of O-heterocycle, alkene, and aldehyde formation in alkane oxidation.[6−16] The complexity of possible isomerization pathways in higher hydrocarbon radical reactions leads naturally to an effort to build general models on the basis of simpler, more easily characterized systems.

In addition to reactions 1a−d, which describe at the molecular level the primary reactive pathways, there are a number of secondary pathways that occasionally contribute. In particular, the QOOH species can also decompose via CO bond fission to again yield HO_2 plus an alkene

$$QOOH \leftrightarrow \text{alkene} + HO_2 \quad (1e)$$

but with a barrier that generally exceeds that for OH loss. At higher temperatures, the direct abstraction of an H atom by O_2 to again yield an alkene + HO_2

$$R + O_2 \rightarrow \text{alkene} + HO_2 \quad (1f)$$

can become significant. It is also worth noting that, in some instances, the HO_2 coproducts may be cyclic hydrocarbons rather than alkenes. Hydrogen transfer from the alpha carbon in RO_2 also produces OH directly

$$RO_2 \rightarrow \text{aldehyde} + OH \quad (1g)$$

but the barrier for this transfer is generally greater than those involved in at least one of the $RO_2 \rightarrow$ QOOH → O-heterocycle + OH pathways.

Reactions 1a−g provide a fairly complete description of the energetically accessible molecular pathways for the R + O_2 system. However, to obtain a complete phenomenological kinetic model for the R + O_2 system that properly reproduces the results of master equation simulations incorporating the

* To whom correspondence should be addressed. E-mail: cataatj@sandia.gov.

10.1021/jp0221946 CCC: $25.00
Published on Web 05/13/2003

above pathways, one must also include rate equations for pathways that would be considered as multistep in nature at the molecular level. In particular, one must include reactions from the reactants to each of the unimolecular and bimolecular products, from each of the unimolecular species to every other one, and from each of the unimolecular species to the bimolecular products. For the R + O_2 system, this implies that, in addition to reactions 1a−g, one must also consider the reactions

$$R + O_2 \rightarrow \text{alkene} + HO_2 \quad (1h)$$

$$R + O_2 \rightarrow \text{O-heterocycle} + OH \quad (1i)$$

$$R + O_2 \rightarrow \text{aldehyde} + OH \quad (1j)$$

$$QOOH_i \leftrightarrow QOOH_j \quad (1k)$$

$$RO_2 \rightarrow \text{O-heterocycle} + OH \quad (1l)$$

$$QOOH \rightarrow \text{aldehyde} + OH \quad (1m)$$

In reaction 1k, the *i* and *j* subscripts denote separate QOOH species, and each of the QOOH reactions should be repeated for each separate QOOH species.

Channel 1h is distinct from channel 1f in that it treats the component that passes through the RO_2 complex. This channel, and similarly the direct OH forming channels 1i and 1j, are of key importance as they provide the mechanism for prompt formation of bimolecular products. These direct steps can dominate kinetically over the corresponding sequential paths.

The ethyl (C_2H_5) + O_2 system is the most thoroughly studied of the alkyl + O_2 reactions both experimentally[2,4,5,12,13,16−24] and theoretically.[24−35] The reaction of ethyl radical with O_2 has been treated as a prototype for the R + O_2 systems, because it is the smallest system in which alkene formation and isomerization to QOOH are possible. Channels 1a and (1b + 1h) dominate the reaction in the temperature region of 296−753 K. At ambient temperature, reactions 1a (addition of O_2 to form the collisionally stabilized ethylperoxy radical) and 1h ("direct" formation of HO_2 + ethene) are the most significant channels.[17,19−21,23] The branching to ethene + HO_2 displays a pressure dependence of $P^{-0.8}$ at 298 K.[21] Ethene formation becomes more significant, and the pressure dependence of the yield becomes less pronounced, as the temperature is increased.[17,19,20] Further, the observed yield of HO_2 and ethene increases sharply with increased temperature in the "transition region," between 500 and 700 K. By 700 K, formation of HO_2 + ethene accounts for nearly 100% of the reaction products.[17,19] The increased formation of alkene at temperatures above 500 K is attributable to the onset of thermal decomposition of the adduct ($C_2H_5O_2$). Earlier master equation simulations[29,30] have shown that this decomposition will produce the final products alkene and HO_2 by two pathways: indirectly, by producing C_2H_5 + O_2 and then having the C_2H_5 product react with O_2 again, and directly, by HO_2 elimination from the thermally reactivated $C_2H_5O_2$*. Recent experiments by Kaiser have demonstrated that both processes occur in the transition region.[19] Experimental and theoretical investigations show that HO_2 production in the propyl + O_2 reaction is similar to that in the ethyl + O_2 reaction.[3,6,10,36−39]

Previous experimental measurements of channels 1d (or 1i) and 1g (or 1j) in the C_2H_5 + O_2 reaction agree that they are minor reaction channels in the temperature range of 296−800 K.[12,13,17,19] Kaiser[19] has recently observed that the total yield of ethylene oxide increased nearly exponentially with increasing temperature from ∼0.1% at 500 K to 2.5% at 660 K. Baldwin et al.[12] also measured the initial product formation of ethylene relative to ethylene oxide [C_2H_4]/[C_2H_4O] to be 127 at 673 K. This ratio is observed to decrease slightly with increased temperature ([C_2H_4]/[C_2H_4O] = 87 at 813 K). Correlating measurements of acetaldehyde with branching into channel 1g (or 1j) is made complicated at lower temperature because CH_3-CHO is also an end product of reactions of $C_2H_5O_2$, and $C_2H_5O_2$ (pathway 1a) is the dominant product of C_2H_5 + O_2 at temperatures below 500 K. At 773 K, Baldwin et al.[12] estimate a lower limit of the initial value for [C_2H_4]/[CH_3CHO] of 1950−2500.

While C_2H_5 + O_2 is considered the "prototype" alkyl + O_2 reaction, larger alkyl + O_2 reactions produce less alkene and more of the OH product channels (with, accordingly, more QOOH) at elevated temperature. The review by Walker and Morley[16] reports initial alkene yields for alkyl radical + O_2 reactions at 753 K and 70 Torr O_2 of 99% for ethyl + O_2, 99% for *t*-C_4H_9 + O_2, 80% for C_3H_7 + O_2, 60% for C_4H_9 + O_2, and 50% for C_5H_{11} + O_2. Epoxides or other cyclic ether species are the stable reaction products of the OH producing pathways in R + O_2 reactions. Since these channels arise from isomerizations to the chain-branching species QOOH, they are of particular interest in modeling ignition phenomena. Given the relative reported epoxide yields for ethyl and propyl reactions with O_2 (∼0.01 and 0.068 at 753 K),[6,12] it is expected that more OH should be observed from propyl + O_2 and that propyl oxidation may better serve as a prototypical system for $RO_2 \leftrightarrow$ QOOH isomerization.

In the current work, the time-resolved production of OH in the propyl + O_2 and ethyl + O_2 systems is studied with a combination of experiment, theory, and modeling. The time-resolved OH formation in pulsed-photolytic Cl-initiated ethane and propane oxidation is observed at a total density of 3.65×10^{17} cm^{-3} and several different temperatures (296, 540, 600, 670, and 700 K) by using laser-induced fluorescence (LIF). These temperatures span the temperature region in which the mechanism changes from being dominated by RO_2 formation to forming ∼100% bimolecular products. LIF of OH ($A^2\Sigma^+ \leftarrow X^2\Pi$) has been used previously by Hughes et al.[40] to observe OH formation from the neopentyl + O_2 reaction. Davidson et al.[41] observed time-resolved OH concentrations for *n*-propane, *n*-butane, *n*-heptane, and *n*-decane oxidation in a shock tube by using laser absorption on the OH $A^2\Sigma^+ \leftarrow X^2\Pi$ (0,0) $R_1(5)$ transition. However, that study is at much higher temperature (between 1550 and 1687 K) and pressure (∼1700 Torr) than the present work.

The observed time-resolved formation of OH is compared with the predictions of an integrated rate equation model for OH formation in the Cl initiated oxidation systems. The central portion of the rate equation models, i.e., that for the R + O_2 systems, is obtained from a parameterization of extended versions of our prior master equation models for these systems. Several parameterizations of alkyl + O_2 reaction systems have been proposed previously. The end product measurements of Walker and co-workers[6−16] rely on an inferred kinetic mechanism and thereby produce Arrhenius parameters for phenomenological reaction steps. Wagner et al.[24,42] generated a phenomenological model for channels 1a and 1b in the ethyl + O_2 reaction as a function of temperature and pressure, using RRKM calculations and a modified strong-collision treatment of stabilization. The transition state characteristics were adjusted to match available kinetic data, including time-resolved

measurements of ethyl disappearance and ethene formation. Wagner et al.[24] assumed that isomerization to C_2H_4OOH preceded formation of ethene + HO_2 products. Bozzelli and Dean[33] presented a QRRK-based model that employed similar assumptions. However, since that early work, direct elimination has been established as the principal means of HO_2 formation,[26,30,31] and the mechanism of the R + O_2 reactions has undergone a fundamental reinterpretation.

Recently, Miller et al.[30] have used master-equation simulations, with ab initio characterization of relevant stationary points, to predict rate constants and branching fractions for the C_2H_5 + O_2 reaction over a wide temperature and pressure range. These calculations have also been used to parameterize the rate constants for channels 1a, 1b, 1f, and 1h as a function of temperature and pressure.[29,30] This parameterized model agrees well with experimental observations of major products. However, the previous model does not provide a parameterization for OH-forming product channels, nor for the formation or decomposition of QOOH. Related master equation simulations have been shown to predict well the experimentally observed forward rate of the propyl + O_2 reaction, as well as the observed time-resolved formation of HO_2 in the temperature region of 296−750 K;[39] however, results for OH and QOOH production have not been previously reported, nor have predictions from the time dependent master equations been previously parameterized.

The present study presents a parameterization of master-equation simulations for the ethyl + O_2 and propyl + O_2 reactions in the temperature region of 296−700 K, including the minor reaction pathways that lead to OH formation, and uses these results to interpret new and previous experimental observations. Parameterizations valid to higher temperature (2000 K), and at constant pressure rather than density, are provided in the Supporting Information. Minor adjustments of the energies of the stationary states have been made, well within the estimated uncertainty of the quantum chemical calculations, to produce the best overall match with experiment. A similar parameterization has recently been presented by Sheng et al.[35] for only the ethyl + O_2 reaction. However, their work employs a time-independent solution of the master equation to produce a rate model, which necessarily entails physically incorrect simplifications. In contrast, the present parameterization employs the well-defined and physically motivated procedure for generating phenomenological rate models from the time-dependent master equation solution described in ref 43.

The resulting phenomenological model for the R + O_2 system is coupled with experimental (where available) and empirical estimates for the reactions of other species (Cl, R, RO_2, QOOH, CCl_2F, RO, OH, HO_2, and O_2QOOH). The overall models do an excellent job of describing the time dependence and the amplitude of HO_2 formation from the Cl initiated oxidation of both ethane and propane. For both systems, the model underpredicts the amount of OH observed at high temperatures (>600 K) and overpredicts the amount of OH observed at lower temperatures (≤600 K). The predicted OH concentrations are also observed to be sensitive to the some of the secondary reactions.

Methods

Experiment. The production of OH in the ethyl + O_2 and propyl + O_2 reactions is monitored by using a pulsed laser photolysis/pulsed laser-induced fluorescence (LP/LIF) method. As in previous investigations of product formation in R + O_2 reactions,[17,19−21,36−39,44] the present experiments utilize Cl-initiated oxidation to study the alkyl + O_2 reactions. The Cl is generated by photolysis at 193 nm of CCl_3F, and the desired alkyl radical is generated by subsequent Cl abstraction from the alkane (either ethane or propane). The alkyl radical then reacts with O_2

$$CCl_3F \xrightarrow{h\nu\ (193\ nm)} Cl + CFCl_2 \quad (2)$$

$$Cl + RH \rightarrow R + HCl \quad (3)$$

$$R + O_2 \rightarrow \text{products} \quad (1)$$

The OH radical is detected at various delay times relative to the photolysis pulse, by LIF following excitation of the OH $A^2\Sigma^+ \leftarrow X^2\Pi$ (1,0) $Q_1(1.5)$ transition at 281.996 nm. The probe laser (7 ns pulse) and the photolysis laser (12 ns pulse) counterpropagate through the cell. The fluorescence is detected perpendicular to the laser beams with a photomultiplier tube, and the time profile of the emitted fluorescence is measured. A UV filter is placed between the photomultiplier tube and the reactor to remove stray probe and photolysis light. The OH fluorescence is integrated over a narrow (30 ns) gate delayed by ∼10 ns from the end of the probe laser pulse. By adjusting the delay of the probe laser with respect to the photolysis pulse, a time profile of the OH LIF signal is obtained. The fluorescence signal is scaled by the probe laser power and corrected for effects of quenching using the directly measured OH fluorescence decay time. The observed fluorescence decay times are very similar for the methanol and alkane reaction systems. The use of narrow-gate detection soon after the excitation pulse minimizes the effects of quenching on the integrated fluorescence[45] and uncertainties in the small residual quenching correction make a negligible contribution to the overall uncertainty.

The experiments are performed in a resistively heated stainless steel flow reactor, where the gas flow is slow compared to the reaction time scale, but high enough to prevent the build up of products. The temperature of the cell is monitored by a retractable thermocouple placed inside the cell directly over the reaction zone. Gas flows are controlled by calibrated mass flow meters, and the pressure in the reactor is monitored with a capacitance manometer. Typical gas concentrations are $[O_2] = 6.3 \times 10^{15}$ cm^{-3}, $[CCl_3F] = 7.6 \times 10^{14}$ cm^{-3}, and $[C_2H_6] = 9 \times 10^{14}$ cm^{-3} or $[C_3H_8] = 5 \times 10^{14}$ cm^{-3}. The methanol reference experiments are performed with $[CH_3OH] = 8 \times 10^{14}$ cm^{-3}, $[NO] = 1.8 \times 10^{15}$ cm^{-3}, $[O_2] = 6.3 \times 10^{15}$ cm^{-3}, and $[CCl_3F] = 7.6 \times 10^{14}$ cm^{-3}. Helium is added to a total density of 3.25×10^{17} cm^{-3}.

The OH signal produced by the R + O_2 reaction is scaled by comparison with the OH signal from the $CH_2OH/O_2/NO$ system under identical photolysis conditions. The CH_2OH is produced by Cl abstraction of hydrogen from methanol[46,47]

$$CCl_3F \xrightarrow{h\nu\ (193\ nm)} Cl + CCl_2F \quad (2)$$

$$CH_3OH + Cl \rightarrow CH_2OH + HCl\ 100\% \quad (4)$$

$$CH_2OH + O_2 \rightarrow CH_2O + HO_2\ 100\% \quad (5)$$

$$HO_2 + NO \xrightarrow{100\%} OH + NO_2 \quad (6)$$

The OH signal obtained from the reference reaction is modeled to account for OH removal reactions, using an integrated rate equation approach. The reactions used in the model for this reference system are listed in Table 1. Figure 1 shows the OH

TABLE 1: Reactions and Rate Coefficients Used to Model the OH Signal Generated from the $Cl/CH_3OH/O_2/NO$ System[a]

reaction	A^b	n	E_a/R (K)	ref
$CH_3OH + Cl \rightarrow HCl + CH_2OH$	5.4×10^{-11}			46
$CH_2OH + O_2 \rightarrow HO_2 + CH_2O$	3.77×10^{-15}	5.94	−2284	55
$HO_2 + NO \rightarrow OH + NO_2$	3.5×10^{-12}		−250	46
$HO_2 + HO_2 \rightarrow O_2 + H_2O_2$[c]	2.2×10^{-13}		−599	47
$OH + HO_2 \rightarrow H_2O + O_2$	4.8×10^{-11}		−250	47
$OH + CH_3OH \rightarrow CH_2OH + H_2O$	2.12×10^{-13}	2.65	−444	56
$OH + NO + M \rightarrow HNO_2 + M$	9.58×10^{-31}	−2.30	−124	57
$OH + OH \rightarrow O + H_2O$	7.89×10^{-14}	2.60	−945	47
$OH + OH + M \rightarrow M + H_2O_2$	6.89×10^{-31}	−0.80		47
$OH + CH_2O \rightarrow HCO + H_2O$	4.73×10^{-12}	1.18	−225	58
$OH + HCO \rightarrow CO + H_2O$	1.70×10^{-10}			58
$OH + NO_2 \rightarrow HNO_3$	2.60×10^{-30}	−2.90		47
$OH + HNO_2 \rightarrow H_2O + NO_2$	6.24×10^{-12}	1	68	57
$HCO + O_2 \rightarrow HO_2 + CO$	5.63×10^{-12}			59
$NO + CH_2OH \rightarrow CH_2OH(NO)$	2.50×10^{-11}			60

[a] Rate coefficients are written in the form $A(T/298)^n e^{-E_a/RT}$. [b] Units of cm^3 molecule^{-1} s^{-1} for second-order reactions and cm^6 molecule^{-2} s^{-1} for third-order reactions. [c] Rate constant has a pressure dependent term; $k = 4.5 \times 10^{-32}$ [M] $+ 2.2 \times 10^{-13} e^{(599K/T)}$.

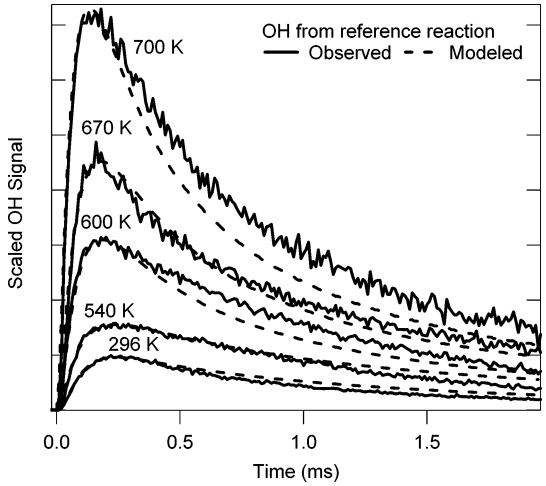

Figure 1. OH time trace from the reference reaction $Cl/CH_3OH/O_2/NO$ at several different temperatures. The observed OH time traces are scaled to match modeled OH signals that are obtain from an integrated rate equation method using the rate coefficients listed in Table 1. The signal and model amplitudes have been scaled for easier comparison.

signals from the reference reaction for five different temperatures; 296, 540, 600, 670, and 700 K. Initial radical concentrations are calculated, using the literature cross-section for CCl_3F at 193 nm, the measured 193 nm laser power, and an assumed photolysis quantum yield of 1, to be from 5 to 9×10^{13} cm^{-3}. Changing the radical density by the estimated uncertainty of ±30% changes the predicted peak $[OH]/[Cl]_0$ ratio inversely by ~8−10%. As seen in Figure 1, the model accurately predicts the observed OH formation rate at each temperature, but more poorly describes the decay of the observed signal. Since getting a reliable estimate of the peak height and hence the radical conversion is the major concern of this model, the literature reaction rate constants are used without alteration. Changing the individual literature rate coefficients within their estimated uncertainties changes the predicted $[OH]/[Cl]_0$ ratio by up to 10%. The fitted OH signals in the reference reaction system, displayed in Figure 1, correspond to a peak OH concentration of between 0.32 and 0.58 × $[Cl]_0$, depending on the temperature and radical concentration in each individual trial.

The ratio of the peak OH concentration, $[OH]_{pk}$, to initial Cl concentration, $[Cl]_0$, predicted by the model is then used to scale the observed OH signal from the Cl-initiated alkane oxidation ($I_{OH}(t)$) as follows

$$\text{Scaled } ([OH](t)) = \frac{I_{OH}(t)}{I_{pk,ref}}\left(\frac{[OH]_{pk}}{[Cl]_0}\right)_{model} \cong \frac{\alpha[OH]_t^{R+O_2}}{\alpha[OH]_{pk,ref}}\frac{[OH]_{pk,ref}}{[Cl]_0} \cong \frac{[OH]_t^{R+O_2}}{[Cl]_0} \quad (7)$$

where $I_{pk,ref}$ is the peak amplitude of the OH signal from the reference reaction, and α is an instrumental proportionality constant. Because the OH signals are corrected for different quenching environments using the measured fluorescence decay and for changes in probe laser power, this proportionality constant is assumed equal for the two reactions. Table 2 lists the scaled peak amplitude of the OH signal derived from eq 7 for both $C_2H_5 + O_2$ and $C_3H_7 + O_2$ at several temperatures. The peak of the scaled OH signal is not a direct measure of the OH branching fraction as the OH radicals are removed at a significant rate compared to their formation. The observed OH signals are modeled as described below using parameterized master equation results for OH production and literature values for other significant OH loss and formation reactions for the R + O_2 system. The overall uncertainty in the scaled amplitudes is a convolution of the propagated uncertainties in the kinetic modeling of the reference reaction, in the estimate of the initial radical density, and in the individual amplitude determinations.

Theory of the R + O_2 System. The master equation simulations have been performed as described in previous work on ethyl + O_2 and propyl + O_2, using the stationary point energies calculated in previous works,[29,30,39] which are summarized here and displayed in Figures 2 and 3. Current theory is in agreement that the $C_2H_5 + O_2$ reaction proceeds through

TABLE 2: Peak Intensity of the Observed OH Signal, the Peak Intensity of the Modeled Reference OH Signal, and the Observed OH Signal Scaled by eq 6 for Both $C_2H_5 + O_2$ and $C_3H_7 + O_2$ at Several Different Temperatures[a]

	T (K)	$I_{pk,R+O_2}/I_{pk,ref}$	$([OH]_{pk,ref}/[Cl]_0)_{model}$[b]	$[OH]_{pk,R+O_2}/[Cl]_0$	$([OH]_{pk}/[Cl]_0)_{model}$
$C_2H_5 + O_2$:	296	0.00023(8)	0.58	0.00014(6)	0.00038
	540	0.0022(6)	0.48	0.0011(4)	0.0017
	600	0.005(1)	0.46	0.0022(9)	0.0025
	670	0.023(3)	0.37	0.008(2)	0.0043
	700	0.035(4)	0.32	0.011(3)	0.0049
$C_3H_7 + O_2$:	296	.00061(8)	0.49	0.00030(8)	0.00073
	530	.007(2)	0.44	0.003(1)	0.0055
	600	.014(4)	0.41	0.006(2)	0.0097
	670	0.041(5)	0.40	0.016(4)	0.016
	700	0.071(9)	0.33	0.023(9)	0.021

[a] The number in parentheses represents the estimated experimental uncertainty in the final digit. The predicted peak OH concentration from the full kinetic model, employing the time-dependent master equation solution for the R + O_2 system, is given in the final column. [b] Estimated uncertainty ± 15%.

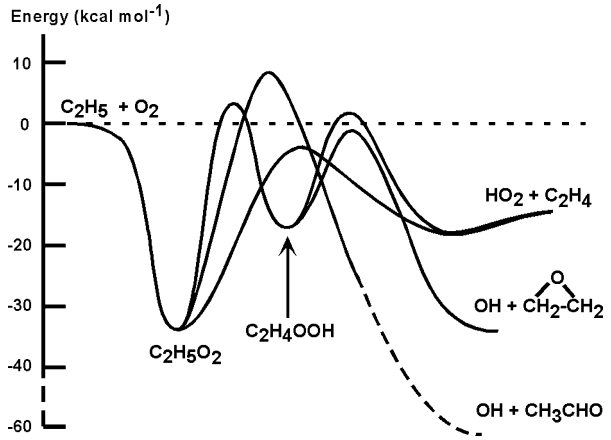

Figure 2. Schematic potential energy surface for the reaction of C_2H_5 with O_2, using calculated stationary point energies from refs 29 and 30.

a barrierless addition pathway to form the adduct $C_2H_5O_2$. The stabilized adduct is calculated[29,30] to be 33.9 kcal mol^{-1} below the reactants. Channel 1b proceeds via concerted elimination of HO_2 from the $C_2H_5O_2$ with an energy barrier 3 kcal mol^{-1} below the reactants. The transition state for channel 1g, corresponding to the elimination of OH via a four membered COOH ring transition state, lies 8.2 kcal mol^{-1} above the reactants. The isomerization of the $C_2H_5O_2$ to C_2H_4OOH via a 1,4 hydrogen shift has a barrier of 3.1 kcal mol^{-1} measured relative to the reactants. This C_2H_4OOH can then decompose at higher temperatures to either $C_2H_4 + HO_2$ or $C_2H_4O + OH$. The calculated barriers to formation of $C_2H_4 + HO_2$ or $C_2H_4O + OH$ from C_2H_4OOH are 1.9 and −0.6 kcal mol^{-1}, respectively (as measured from the energy of reactants). The barrier for direct abstraction to produce $C_2H_4 + HO_2$ is 18.2 kcal mol^{-1} above reactants.

The primary pathway to HO_2 formation in the *n*-propyl and *i*-propyl + O_2 reactions is again concerted elimination of HO_2 from the $C_3H_7O_2$.[32,39,48] The elimination transition state lies 5.2 kcal mol^{-1} and 7.0 kcal mol^{-1} below the reactants for *n*-C_3H_7 and *i*-C_3H_7, respectively.[39] The 1,4 hydrogen shift to form QOOH is calculated to be 2.6 and 1.4 kcal mol^{-1} below the reactants for *n*-$C_3H_7 + O_2$ and *i*-$C_3H_7 + O_2$, respectively. The barrier to products from *n*-C_3H_6OOH is 6.5 and 3.4 kcal mol^{-1} below the reactants for OH and HO_2 formation, respectively, and 4.9 and 1.9 kcal mol^{-1} below the reactants for OH and HO_2 formation from *i*-C_3H_6OOH. The *n*-$C_3H_7O_2$ radical has another possible isomerization, the 1,5 hydrogen shift to form $CH_2CH_2CH_2OOH$. This isomerization has a much lower barrier, 11.2 kcal mol^{-1} below reactants, but $CH_2CH_2CH_2OOH$ has a sizable barrier to formation of either OH or HO_2.[39] The barriers to formation of CH_3CHCH_2 via direct abstraction are at 16.1 and 13.0 kcal mol^{-1} relative to reactants for *n*-propyl and i-propyl, respectively.

For ethyl + O_2, the barrier heights, and indeed the full model, are precisely as described in our earlier work.[29,30] This model directly employs the ab initio thermochemical data for all but the $C_2H_5O_2$ well depth, which was decreased by 0.4 kcal/mol. For propyl + O_2, the present inclusion of tunneling corrections, which were neglected in our prior study that focused on the HO_2 elimination channels, necessitated further minor revision of the energetics. In particular, for *n*-propyl, the transition state for elimination of HO_2 from $CH_3CH_2CH_2OO$ is now raised by 1.4 instead of 1.0 kcal mol^{-1} and the transition state for isomerization from $CH_3CH_2CH_2OO$ to CH_3CHCH_2OOH is now

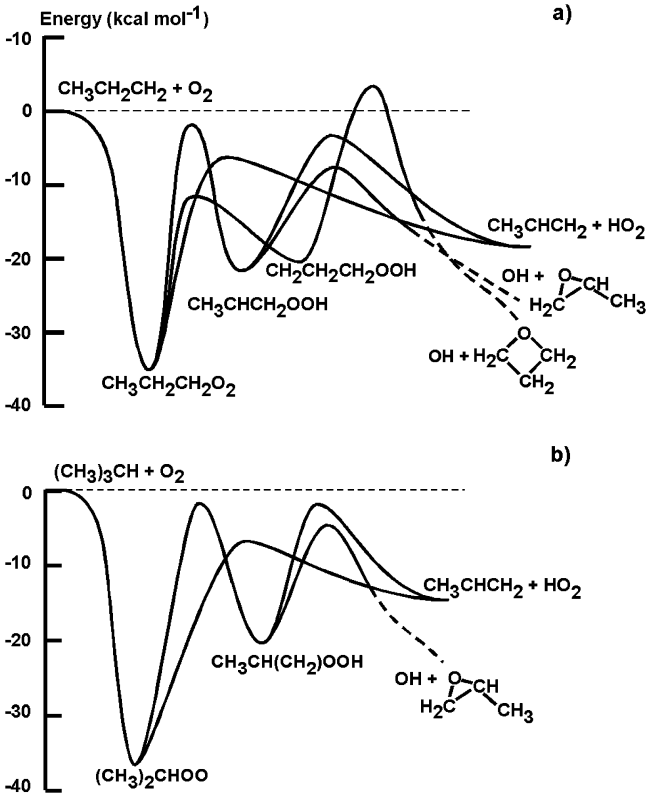

Figure 3. Schematic potential energy surfaces for the reactions of (a) *n*-C_3H_7 with O_2 and (b) *i*-C_3H_7 with O_2, using calculated stationary point energies from ref 39.

raised by 0.5 kcal mol^{-1} from the ab initio value (instead of being lowered by 1.0 kcal mol^{-1}). For *i*-propyl, the transition state for elimination of HO_2 from $CH_3CH(CH_3)OO$ is now raised by 2.3 instead of 2.0 kcal mol^{-1} and the transition state for isomerization from $CH_3CH_2CH_2OO$ to CH_3CHCH_2OOH is now raised by 1.2 kcal mol^{-1} instead of being lowered by 0.5 kcal mol^{-1}. With these changes, the comparison between the master equation predictions and experiment remains essentially identical to that described in ref 39.

For channels with a well-defined saddlepoint, the microcanonical rate coefficients have been evaluated on the basis of conventional transition state theory. Various low frequency modes have been treated as one-dimensional hindered rotors generally using quantum-chemical evaluations of all of the minima to generate a Fourier representation of the potential surface. Such torsional potentials are then employed in Pitzer-Gwinn[49] based evaluations of the partition functions and sums and densities of states. One-dimensional tunneling corrections employing asymmetric Eckart potentials are included and the remaining modes are treated with rigid-rotor harmonic oscillator assumptions.

For the barrierless entrance channel, variable reaction coordinate transition state theory is employed. For propyl + O_2,[39] the requisite transitional modes potential is based on ab initio quantum evaluations at the B3LYP/6-31G* level of the energies along the minimum energy path. The force field for the transitional bending modes consisted of sums of sinusoidally hindered rotors, with an exponential decay of the force constants with separation. The relative magnitude of the force constants for different modes is adjusted to reproduce the calculated values at the equilibrium adduct geometry. The absolute magnitude and decay of such force constants is adjusted to reproduce previous observed experimental high-pressure rate constants.

TABLE 3: Parameterized Rate Coefficients and Equilibrium Constants for the $C_2H_5 + O_2$ System Generated from Solutions to the Master Equation[a]

reaction	A^b	n	E_a/R (K)	k_{675K}
$C_2H_5 + O_2 \rightarrow C_2H_5O_2$	1.95×10^{-8}	−9.22	2630	2.11×10^{-13}
$C_2H_5 + O_2 \rightarrow C_2H_4OOH$	6.65×10^{-13}	−8.62	2430	1.58×10^{-17}
$C_2H_5 + O_2 \rightarrow C_2H_4 + HO_2$	1.61×10^{-12}	−1.87	707	1.22×10^{-13}
$C_2H_5 + O_2 \rightarrow C_2H_4O + OH$	1.82×10^{-15}	−0.09	404	9.29×10^{-16}
$C_2H_5 + O_2 \rightarrow CH_3CHO + OH$	4.31×10^{-20}	7.74	−1400	1.92×10^{-16}
$C_2H_5O_2 \rightarrow C_2H_4 + HO_2$	8.66×10^{14}	−6.88	17060	33.0
$C_2H_{55}O_2 \rightarrow C_2H_4O + OH$	2.00×10^{18}	−15.61	21910	0.0458
$C_2H_5O_2 \rightarrow CH_3CHO + OH$[c]	2.63×10^{12}	−9.84	19030	4.92×10^{-4}
	5.70×10^{-3}	6.75	7930	
$C_2H_4OOH \rightarrow C_2H_5O_2$	1.41×10^{6}	−0.229	3620	5480
$C_2H_4OOH \rightarrow C_2H_4 + HO_2$	2.17×10^{14}	−8.69	10680	23900
$C_2H_4OOH \rightarrow C_2H_4O + OH$	8.27×10^{14}	−8.29	9950	373000
$C_2H_4OOH \rightarrow CH_3CHO + OH$	9.16×10^{5}	−6.73	9550	2.68×10^{-3}
K_{eq} $C_2H_5 + O_2 \rightleftharpoons C_2H_5O_2$	7.73×10^{-28}	1.45	−17670	5.91×10^{-16}
K_{eq} $C_2H_5 + O_2 \rightleftharpoons C_2H_4OOH$	2.12×10^{-27}	1.94	−9210	8.73×10^{-21}
K_{eq} $C_2H_4OOH \rightleftharpoons C_2H_5O_2$	0.365	−0.49	−8460	67800

[a] The rate coefficients are expressed as $k = A(T/298)^n e^{-E_a/RT}$. [b] Units cm^3 $molecule^{-1}$ s^{-1} for second-order reactions, s^{-1} for first-order reactions, cm^3 for unimolecular/bimolecular equilibria, and dimensionless for unimolecular/unimolecular equilibria. [c] For this reaction, the rate coefficient is expressed as the sum of the two modified Arrhenius forms.

TABLE 4: Parameterized Rate Coefficients and Equilibrium Constants for the i-$C_3H_7 + O_2$ System Generated from Solutions to the Master Equation[a]

reaction	A^b	n	E_a/R (K)	k_{675K}
i-$C_3H_7 + O_2 \rightarrow i$-$C_3H_7O_2$	1.05×10^{-6}	−11.1	3290	9.18×10^{-13}
i-$C_3H_7 + O_2 \rightarrow i$-$C_3H_6OOH$	6.21×10^{-11}	−9.37	2790	4.69×10^{-16}
i-$C_3H_7 + O_2 \rightarrow i$-$C_3H_6 + HO_2$	3.75×10^{-11}	−3.02	1260	4.91×10^{-13}
i-$C_3H_7 + O_2 \rightarrow i$-$C_3H_6O + OH$	6.16×10^{-13}	−1.87	1140	2.47×10^{-14}
i-$C_3H_7 + O_2 \rightarrow i$-$C_2H_5CHO + OH$	6.95×10^{-17}	3.04	−190	1.11×10^{-15}
i-$C_3H_7O_2 \rightarrow i$-$C_3H_6 + HO_2$	9.38×10^{16}	−7.86	18430	211
i-$C_3H_7O_2 \rightarrow i$-$C_3H_6O + OH$	1.45×10^{19}	−13.2	21750	3.02
i-$C_3H_7O_2 \rightarrow i$-$C_2H_5CHO + OH$[c]	16.3	3.34	9390	1.17×10^{-2}
	4.73×10^{24}	−25.4	27350	
i-$C_3H_6OOH \rightarrow i$-$C_3H_7O_2$[c]	1.28×10^{6}	−2.30	3870	9.23×10^{3}
	8.61×10^{13}	−10.1	9970	
i-$C_3H_6OOH \rightarrow i$-$C_3H_6 + HO_2$	4.11×10^{15}	−9.09	11400	1.13×10^{5}
i-$C_3H_6OOH \rightarrow i$-$C_3H_6O + OH$	1.12×10^{15}	−7.54	9500	1.82×10^{6}
i-$C_3H_6OOH \rightarrow i$-$C_2H_5CHO + OH$	1.70×10^{8}	−6.91	10960	5.31×10^{-2}
K_{eq} i-$C_3H_7 + O_2 \rightleftharpoons i$-$C_3H_7O_2$	2.90×10^{-29}	2.03	−19500	5.36×10^{-16}
K_{eq} i-$C_3H_7 + O_2 \rightleftharpoons i$-$C3H_6OOH$	2.29×10^{-27}	2.56	−10830	1.73×10^{-19}
K_{eq} i-$C_3H_6OOH \rightleftharpoons i$-$C_3H_7O_2$	1.25×10^{-2}	−0.52	−8670	3090

[a] The rate coefficients are expressed as $k = A(T/298)^n e^{(-E_a/RT)}$. [b] Units cm^3 $molecule^{-1}$ s^{-1} for second-order reactions, s^{-1} for first-order reactions, cm^3 for unimolecular/bimolecular equilibria, and dimensionless for unimolecular/unimolecular equilibria. [c] For these reactions, the rate coefficient is expressed as the sum of the two modified Arrhenius forms.

A related, but more empirical, transitional mode potential was employed for the ethyl + O_2 case, as described in our earlier work.[29,30]

An exponential down model is employed for the energy transfer process. For ethyl + O_2, a temperature independent value of $\Delta E_{down} = 200$ cm^{-1} was employed, again as in our prior work.[29,30] For propyl + O_2, a value of 350 cm^{-1} was instead employed, again independent of temperature. Improved agreement with experiment could be obtained by employing ΔE_{down} values that increase with temperature, but related studies suggest that such a temperature dependence is unphysical.[50] The one-dimensional time-dependent master equation is solved via diagonalization of the transition matrix. The VARIFLEX[51] software was used in these master equation simulations.

The results of the time-dependent master equation analysis of ethyl + O_2 have been previously reduced to a set of elementary reactions and phenomenological rate coefficients for HO_2 formation.[29] These predicted rate coefficients for channels 1a, 1b, 1f, and 1h as a function of both temperature and pressure were designed to be used in modeling of the reaction. A new set of rate coefficients is obtained in the present work from the time-dependent master equations for both ethyl and propyl + O_2, including pathways describing the OH formation as a function of temperature at the density of the experiments. The phenomenological rate constants are obtained from the solutions to the master equations at 296, 350, 400, 470, 540, 600, 670, 700, and 750 K using the methodology described in ref 43. The change of these phenomenological rate coefficients with temperature are then fit to modified Arrhenius equations, with maximum fitting errors of 20%.

The modified Arrhenius parameters describing the temperature-dependent phenomenological rate coefficients for $C_2H_5 + O_2$ are listed in Table 3, for i-$C_3H_7 + O_2$ in Table 4, and for n-$C_3H_7 + O_2$ in Table 5. These parameterizations are valid at the total density of the present experiments (3.65×10^{17} cm^{-3}) and the temperature range 296−750 K. For reference purposes, related constant pressure parameterizations (0, 30, 760, 7600 Torr) for the 300−2000 K range are provided as Supporting Information. Figure 4 demonstrates how effective these parameterizations derived from the time-dependent master equation are at reproducing the solutions to the time-dependent master equation for the ethyl + O_2 system at 700 K. As seen in Figure 4, the rate of formation as well as the branching fraction of the three major products for ethyl + O_2 (OH, HO_2, and $C_2H_5O_2$) are reproduced to a high degree of accuracy by the parameterization.

For the n-propyl + O_2 reaction the $CH_2CH_2CH_2OOH$ species reaches its stabilization limit by about 450 K. Above that

TABLE 5: Parameterized Rate Coefficients and Equilibrium Constants for the *n*-C_3H_7 + O_2 System Generated from Solutions to the Master Equation[a]

reaction	A^b	n	E_a/R (K)	k_{675K}
n-$C_3H_7 + O_2 \rightarrow$ *n*-$C_3H_7O_2$	3.47×10^{-8}	−8.23	2600	8.81×10^{-13}
n-$C_3H_7 + O_2 \rightarrow$ *n*-$CH_3CHCH_2O_2H$	9.89×10^{-16}	−3.17	570	3.18×10^{-17}
n-$C_3H_7 + O_2 \rightarrow$ *n*-$C_3H_6 + HO_2$	5.70×10^{-12}	−1.63	1720	1.18×10^{-13}
n-$C_3H_7 + O_2 \rightarrow$ *n*-$C_3H_6O + OH$	9.49×10^{-13}	−1.84	1660	1.80×10^{-14}
n-$C_3H_7 + O_2 \rightarrow$ *n*-$C_2H_5CHO + OH$	2.45×10^{-16}	3.16	1260	5.02×10^{-16}
n-$C_3H_7 + O_2 \rightarrow$ *c*-$CH_2CH_2CH_2O + OH$	3.39×10^{-14}	0.50	2510	1.24×10^{-15}
n-$C_3H_7O_2 \rightarrow$ *n*-$C_3H_6 + HO_2$	2.02×10^{14}	−4.48	16410	143
n-$C_3H_7O_2 \rightarrow$ *n*-$C_3H_6O + OH$	3.98×10^{14}	−6.34	16950	27.7
n-$C_3H_7O_2 \rightarrow$ *n*-$C_2H_5CHO + OH$[c]	6.70×10^{-6}	14.91	5040	5.32×10^{-2}
	1.20×10^{15}	−8.89	20520	
n-$C_3H_7O_2 \rightarrow$ *n*-$CH_2CH_2CH_2O + OH$	6.62×10^{16}	−9.91	21920	0.158
n-$CH_3CHCH_2O_2H \rightarrow$ *n*-$C_3H_7O_2$	9.76×10^{5}	−0.349	4320	1219
n-$CH_3CHCH_2O_2H \rightarrow$ *n*-$C_3H_6 + HO_2$	1.05×10^{14}	−8.52	11020	8050
n-$CH_3CHCH_2O_2H \rightarrow$ *n*-$C_3H_6O + OH$	1.75×10^{15}	−7.82	9450	2.43×10^{6}
n-$CH_3CHCH_2O_2H \rightarrow$ *n*-$C_2H_5CHO + OH$	0.160	6.80	6920	1.47×10^{-3}
n-$CH_3CHCH_2O_2H \rightarrow$ *n*-$CH_2CH_2CH_2O + OH$	8.38×10^{5}	−1.28	12150	4.48×10^{-3}
n-$CH_2CH_2CH_2O_2H \rightarrow$ *n*-$C_3H_7O_2$	2.12×10^{7}	2.51	1040	3.54×10^{7}
n-$CH_2CH_2CH_2O_2H \rightarrow$ *n*-$CH_3CHCH_2O_2H$	179	6.38	2860	477
K_{eq} *n*-$C_3H_7 + O_2 \rightleftharpoons$ *n*-$C_3H_7O_2$	3.72×10^{-28}	1.68	−17940	5.12×10^{-16}
K_{eq} *n*-$C_3H_7 + O_2 \rightleftharpoons$ *n*-$CH_3CHCH_2O_2H$	1.20×10^{-26}	1.47	−11510	1.02×10^{-18}
K_{eq} *n*-$CH_3CHCH_2O_2H \rightleftharpoons$ *n*-$C_3H_7O_2$	3.08×10^{-2}	0.22	−6440	513
K_{eq} *n*-$CH_2CH_2CH_2O_2H \rightleftharpoons$ *n*-$C_3H_7O_2$	0.575	−1.06	−7060	8430
K_{eq} *n*-$CH_2CH_2CH_2O_2H \rightleftharpoons$ *n*-$CH_3CHCH_2O_2H$	18.7	−1.27	−610	16.3

[a] The rate coefficients are expressed as $k = A(T/298)^n e^{(-E_a/RT)}$. [b] Units cm^3 $molecule^{-1}$ s^{-1} for second-order reactions, s^{-1} for first-order reactions, cm^3 for unimolecular/bimolecular equilibria, and dimensionless for unimolecular/unimolecular equilibria. [c] For this reaction, the rate coefficients is expressed as the sum of the two modified Arrhenius forms.

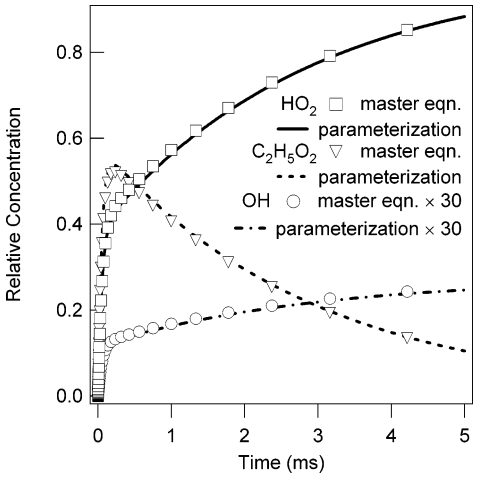

Figure 4. Comparison between the predictions of the time-dependent master equation (symbols) and the integrated rate equations listed in Table 1 (lines) for the reaction of $C_2H_5 + O_2$ at 700 K. Shown is the predicted change in the $[OH]/[C_2H_5]_0$ (circles), $[HO_2]/[C_2H_5]_0$ (squares), and $[C_2H_5O_2]/[C_2H_5]_0$ (triangles) with time. The parameterization accurately reproduces the master equation predictions.

temperature, this isomer, in essence, does not exist as a chemical entity. The procedure[43] for deriving the related phenomenological rate coefficients from the master equation is then inapplicable. Importantly, however, the rate coefficients involving the remaining species can still be obtained by simply considering one less term in the sum over eigenvalues, i.e., one employs the standard expression[43] with the realization that there is one less chemical species. By doing so, the rate for producing products such as $CH_2CH_2CH_2O + OH$ from $CH_2CH_2CH_2OOH$ is subsumed into the rate for producing these products from $CH_3CH_2CH_2OO$. In essence, the $CH_2CH_2CH_2OOH$ species has just become part of the total $CH_3CH_2CH_2OO$ reservoir.

Because the stabilization limit for $CH_2CH_2CH_2OOH$ is so low, i.e., below the majority of the temperatures of interest here, we present no rate coefficients for its coupling with bimolecular species. However, as there is considerable interest in the concentrations of QOOH species such as $CH_2CH_2CH_2OOH$, we do include rate expressions for its unimolecular isomerizations. These expressions are valid only below 450 K. Above that temperature, any reactions of $CH_2CH_2CH_2OOH$ with other species should really be considered as reactions of CH_3CH_2-CH_2OO.

Comprehensive Kinetic Model. The parameterization of the phenomenological rate coefficients for $C_2H_5 + O_2$ and $C_3H_7 + O_2$ derived from the time-dependent master equations allows a model of the reaction systems to be constructed by using the elementary reactions involved in the two reaction systems. The experimentally observed OH time traces can then be compared to predictions of this model. For these parameterizations to reproduce the observed experimental data, rate coefficients must be added to the model that describe the loss and formation of several other radicals involved in the experiment (OH, HO_2, Cl, CCl_2F, R, RO_2, RO, QOOH, and O_2QOOH). Literature rate constants associated with these reactions are combined with the parameterizations to form an integrated rate equation model that describes both OH and HO_2 formation and removal mechanisms important in the time domain of the experiment. The reactions and rate coefficients used in the model are listed in Table 6 for $C_2H_5 + O_2$ and Table 7 for $C_3H_7 + O_2$.

There are several reactions in the model that have not been experimentally studied. The rate constants for these reactions are estimated by using rate constants for similar reactions. Estimates of several of these rate constants are based on similar reactions in the more thoroughly studied CH_3/O_2 system. One of the most important of these reactions is the reaction of the alkyl radical with HO_2, which can form OH + RO. The model uses the estimated rate constant for $CH_3 + HO_2 \rightarrow OH + CH_3O$ of 3×10^{-11} cm^3 $molecule^{-1}$ s^{-1} for all $R + HO_2 \rightarrow OH + RO$ reactions.[52] Zhu and Lin[53] calculate a slightly higher rate constant. For comparison, Bozzelli and Dean[33] estimate a rate coefficient for ethyl + $HO_2 \rightarrow OH + CH_3CH_2O$ to be 4.98×10^{-11} cm^3 $molecule^{-1}$ s^{-1}. Calculations at the B3LYP/6-31G* level indicate that the addition of HO_2 to ethyl is barrierless. Furthermore, variational transition state theory calculations incorporating a transitional mode potential based on fits of a sinusoidally hindered form to the B3LYP/6-31G* calculated

TABLE 6: Reactions and Rate Coefficients Used to Model the OH Signal from the $Cl/C_2H_6/O_2$ System[i]

reaction	A[a]	n	E_a/R (K)	ref
$C_2H_5 + O_2 \rightarrow$ products				Table 3
$C_2H_6 + Cl \rightarrow HCl + C_2H_5$	3.4×10^{-11}	0.7	−150	61
$C_2H_6 + OH \rightarrow C_2H_5 + H_2O$	1.06×10^{-12}	2.06	430	62
$HO_2 + HO_2 \rightarrow O_2 + H_2O_2$[b]	2.2×10^{-13}		−599	47
$OH + HO_2 \rightarrow H_2O + O_2$	4.8×10^{-11}		−250	47
$OH + OH \rightarrow O + H_2O$	7.89×10^{-14}	2.60	−945	47
$OH + OH + M \rightarrow M + H_2O_2$	6.89×10^{-31}	−0.80		47
$C_2H_5O_2 + C_2H_5O_2 \rightarrow 2\ C_2H_5O + O_2$	$\phi \times 8.5 \times 10^{-14}$		125	63[c]
$C_2H_5O_2 + C_2H_5O_2 \rightarrow C_2H_5OH + CH_3CHO$	$(1\text{-}\phi) \times 8.5 \times 10^{-14}$		125	63[c]
$C_2H_5O_2 + HO_2 \rightarrow C_2H_5O_2H + O_2$	6.9×10^{-13}		−702	64
$C_2H_5O_2 + OH \rightarrow HO_2 + C_2H_5O$	1×10^{-11}			*d*
$C_2H_4OOH + O_2 \rightarrow HOOC_2H_4O_2$	$3.98 \times 10\text{-}^{12}$	−0.44		34
$HOOC_2H_4O_2 \rightarrow C_2H_4OOH + O_2$	2.55×10^{16}	−2.45	18270	34
$HOOC_2H_4O_2 \rightarrow OH + HOOCH_2CHO$	1.98×10^{7}	3.27	14432	34
$HOOC_2H_4O_2 \rightarrow OH + HOOCH_2CHO$	1.37×10^{8}	3.19	20260	34
$HOOC_2H_4O_2 \rightarrow OH + OCH_2CH_2OO$	3.0×10^{15}		43500	34
$HOOC_2H_4O_2 \rightarrow HO_2 + HOOCH_2CHO$	4.17×10^{7}	3.51	14822	34
$C_2H_5 + OH \rightarrow C_2H_4 + H_2O$	4.0×10^{-11}			52
$C_2H_5 + C_2H_5 \rightarrow$ products	1.99×10^{-11}			65
$C_2H_5 + C_2H_5O_2 \rightarrow 2C_2H_5O$	4.0×10^{-11}			52[e]
$C_2H_5 + HO_2 \rightarrow OH + C_2H_5O$	3.0×10^{-11}			52[e]
$C_2H_5 + HO_2 \rightarrow O_2 + C_2H_6$	6.0×10^{-12}			52[e]
$C_2H_5 + C_2H_5O \rightarrow (C_2H_5)_2O$	2.0×10^{-12}			66
$C_2H_5O + OH \rightarrow C_2H_4O + H_2O$	3.0×10^{-11}			52[e]
$C_2H_5O + O_2 \rightarrow HO_2 + C_2H_4O$	6.0×10^{-14}		549	47
$C_2H_5O + HO_2 \rightarrow H_2O_2 + C_2H_4O$	5.0×10^{-13}			52[e]
$C_2H_5O + C_2H_5O_2 \rightarrow C_2H_5OOH + C_2H_4O$	5.0×10^{-13}			52[e]
$C_2H_5O + C_2H_5O \rightarrow C_2H_5OH + CH_3CHO$	3.0×10^{-11}			52[e]
$Cl + C_2H_5 \rightarrow HCl + C_2H_4$	7.57×10^{-10}		290	67
$Cl + C_2H_5O_2 \rightarrow ClO + C_2H_5O$	7.4×10^{-11}			68[e]
$Cl + HO_2 \rightarrow ClO + OH$	4.1×10^{-11}		450	47
$Cl + HO_2 \rightarrow HCl + O_2$	1.8×10^{-11}		−170	47
$Cl + C_2H_5O \rightarrow C_2H_4O + HCl$	2.0×10^{-11}			69[e]
$CCl_2F + O_2 \rightarrow CCl_2FO_2$	6.16×10^{-30}	−5.61		70
$CCl_2FO_2 \rightarrow CCl_2F + O_2$	3.47×10^{12}	−2.27	11500	f
$CCl_2F + Cl \rightarrow CCl_3F$	1.0×10^{-10}			71[g]
$CCl_2F + C_2H_5 \rightarrow HCCl_2F + C_2H_4$	4.7×10^{-11}	−0.50		52[e]
$CCl_2F + C_2H_5O_2 \rightarrow C_2H_5O + CCl_2FO$	4.0×10^{-11}			52[e]
$CCl_2F + HO_2 \rightarrow OH + CCl_2FO$	1.4×10^{-12}			*h*
$CCl_2F + HO_2 \rightarrow O_2 + CCl_2FH$	$6. \times 10^{-13}$			*h*
$CCl_2F + OH \rightarrow CCl_2FOH$	5.0×10^{-11}			52[e]
$CCl_2F + C_2H_5O \rightarrow$ products	2.0×10^{-11}			52[e]
$CCl_2F + CCl_2F \rightarrow$ products	1.0×10^{-11}			72[g]

[a] Units of s^{-1} for first-order reactions, cm^3 molecule^{-1} s^{-1} for second-order reactions, and cm^6 molecule^{-2} s^{-1} for third-order reactions. [b] Rate constant has a pressure dependent term; $k = 4.5 \times 10^{-32}$ [M] + $2.2 \times 10^{-13}e^{(599K/T)}$. [c] The branching fraction is fit to the function $\phi = 1.33 \exp(-209/T)$[63]. [d] Estimated on the basis of $CF_3O_2 + OH$.[54] [e] Estimated on the basis of the CH_3/O_2 system.[52] [f] Estimated on the basis of the CCl_3F-O_2 bond energy compared to $C_2H_5-O_2$. [g] Estimated on the basis of the CCl_3/O_2 system. [h] Calculated rate constant. [i] Rate coefficients are written in the form $A(T/298)^n e^{-E_a/RT}$.

force field yield an addition rate constant of 2×10^{-11} cm^3 molecule^{-1} s^{-1}.

The reactions of the ethylperoxy and propylperoxy radicals (RO_2) with OH have not been experimentally studied. However, the reaction

$$CF_3O_2 + OH \rightarrow HO_2 + CF_3O \quad (8)$$

has been experimentally studied and is found to have a significant rate constant (4×10^{-11} cm^3 molecule^{-1} s^{-1}).[54] This is slightly less than half the estimate for the $CH_3O_2 + OH$ rate constant estimated by Tsang and Hampson[52] ($k = 1 \times 10^{-10}$ cm^3 molecule^{-1} s^{-1}) A rate coefficient of 4×10^{-11} cm^3 molecule^{-1} s^{-1} is used for $C_2H_5O_2 + OH$ and *i*-, *n*-$C_3H_7O_2 + OH$. Rate constants that have not been determined experimentally for the C_3H_7/O_2 system are assumed to be identical to the analogous rate constants in the C_2H_5/O_2 system.

The reactions involving the counter radical CCl_2F have not been heavily studied. Rate coefficients for these reactions are estimated based on comparison to analogous reactions in either of the CCl_3/O_2 or CH_3/O_2 systems as indicated in Tables 6 and 7. The $CCl_2F + O_2$ equilibrium is estimated by comparing the B3LYP/6-31G* calculated bond energy of CCl_2F-O_2 to that calculated for $C_2H_5-O_2$. The rate coefficient for the reaction

$$CCl_2F + HO_2 \rightarrow OH + CCl_2FO \quad (9)$$

is estimated by variational transition state theory, again employing a transitional mode potential based on fits to B3LYP/6-31G* energies, to be a factor of 10 lower than that of the ethyl + HO_2 reaction ($k_9 = 2 \times 10^{-12}$ cm^3 molecule^{-1} s^{-1}). This reaction may contribute to OH formation in the present experiments because the competing removal reactions for CCl_2F are also relatively slow.

Results

HO_2 Formation. The first test of the integrated rate equation model is to see how well it reproduces the more abundant product, HO_2. The observed formation of HO_2 from the reaction of ethyl + O_2 and propyl + O_2 has previously been directly compared to predictions of time dependent master equations after correcting for HO_2 removal reactions from the main HO_2 loss mechanisms ($HO_2 + HO_2$ and $HO_2 + RO_2$) using an iterative integration technique.[17,29,30,39] Agreement between these corrected time traces (at total densities of 8.5×10^{17} cm^{-3})

TABLE 7: Reactions and Rate Constants Used to Model the OH Signal Generated from the Cl/C_3H_8/O_2 System[q]

reaction	A[a]	n	E_a/R (K)	ref
i-$C_3H_7 + O_2 \rightarrow$ products				Table 4
n-$C_3H_7 + O_2 \rightarrow$ products				Table 5
$C_3H_8 + Cl \rightarrow HCl + n$-$C_3H_7$	1.12×10^{-10}		212	73
$C_3H_8 + Cl \rightarrow HCl + i$-$C_3H_7$	8.13×10^{-11}		86	73
$C_3H_8 + OH \rightarrow n$-$C_3H_7 + H_2O$	$\phi \times 1.87 \times 10^{-12}$	1.72	145	74[b]
$C_3H_8 + OH \rightarrow i$-$C_3H_7 + H_2O$	$(1\text{-}\phi) \times 1.06 \times 10^{-12}$	1.72	145	74[b]
$HO_2 + HO_2 \rightarrow O_2 + H_2O_2$[c]	2.2×10^{-13}		−599	47
$OH + HO_2 \rightarrow H_2O + O_2$	4.8×10^{-11}		−250	47
$OH + OH \rightarrow O + H_2O$	7.89×10^{-14}	2.60	−945	47
$OH + OH + M \rightarrow M + H_2O_2$	6.89×10^{-31}	−0.80		47
n-$C_3H_7O_2 + n$-$C_3H_7O_2 \rightarrow$ products	5×10^{-13}		150	75
i-$C_3H_7O_2 + i$-$C_3H_7O_2 \rightarrow$ products	1.7×10^{-12}		2190	76[e]
n-$C_3H_7O_2 + i$-$C_3H_7O_2 \rightarrow$ products				*e, f*
n-$C_3H_7O_2 + HO_2 \rightarrow n$-$C_3H_7O_2H + O_2$	6.9×10^{-13}		−702	*g*
i-$C_3H_7O_2 + HO_2 \rightarrow i$-$C_3H_7O_2H + O_2$	6.9×10^{-13}		−702	*g*
n-$C_3H_7O_2 + OH \rightarrow HO_2 + n$-$C_3H_7O$	1×10^{-11}			*h*
i-$C_2H_5O_2 + OH \rightarrow HO_2 + i$-$C_2H_5O$	1×10^{-11}			*h*
$C_3H_6OOH + O_2 \rightarrow HOOC_3H_6O_2$	3.98×10^{-12}	−0.44		*i*
$HOOC_3H_6O_2 \rightarrow C_3H_6OOH + O_2$	2.55×10^{16}	−2.45	18270	*i*
$HOOC_3H_6O_2 \rightarrow OH + HOOC_3H_5O$	1.98×10^{7}	3.27	14432	*i*
$HOOC_3H_6O_2 \rightarrow OH + HOOC_3H_5O$	1.37×10^{8}	3.19	20260	*i*
$HOOC_3H_6O_2 \rightarrow OH + OOC_3H_6O$	3.0×10^{15}		43500	*i*
$HOOC_3H_6O_2 \rightarrow HO_2 + C_3H_6O_2$	4.17×10^{7}	3.51	14822	*i*
n-$C_3H_7 + OH \rightarrow C_3H_6 + H_2O$	4.0×10^{-11}			77
i-$C_3H_7 + OH \rightarrow C_3H_6 + H_2O$	4.0×10^{-11}			77
n-$C_3H_7 + n$-$C_2H_5 \rightarrow$ products	1.7×10^{-11}			77
i-$C_3H_7 + i$-$C_3H_7 \rightarrow$ products	1.0×10^{-11}	−0.70		77
i-$C_3H_7 + n$-$C_3H_7 \rightarrow$ products	2.91×10^{-11}			77
i-$C_3H_7 + i$-$C_3H_7O_2 \rightarrow 2\ i$-$C_3H_7O$	1.66×10^{-11}			78
i-$C_3H_7 + n$-$C_3H_7O_2 \rightarrow i$-$C_3H_7O + n$-C_3H_7O	1.66×10^{-11}			*j*
n-$C_3H_7 + n$-$C_3H_7O_2 \rightarrow 2\ n$-$C_3H_7O$	1.66×10^{-11}			*j*
n-$C_3H_7 + i$-$C_3H_7O_2 \rightarrow i$-$C_3H_7O + n$-C_3H_7O	1.66×10^{-11}			*j*
n-$C_3H_7 + HO_2 \rightarrow OH + n$-$C_3H_7O$	3.0×10^{-11}			*k*
i-$C_3H_7 + HO_2 \rightarrow OH + i$-$C_3H_7O$	3.0×10^{-11}			*k*
n-$C_3H_7 + HO_2 \rightarrow O_2 + n$-$C_3H_8$	6.0×10^{-12}			*k*
i-$C_3H_7 + HO_2 \rightarrow O_2 + i$-$C_3H_8$	6.0×10^{-12}			*k*
$C_3H_7 + C_3H_7O \rightarrow (C_3H_7)_2O$	2.0×10^{-12}			*l*
$C_3H_7O + OH \rightarrow C_3H_6O + H_2O$	3.0×10^{-11}			*k*
i-$C_3H_7O + O_2 \rightarrow HO_2 + i$-$C_3H_6O$	1.6×10^{-14}		264.6	79
n-$C_3H_7O + O_2 \rightarrow HO_2 + n$-$C_3H_6O$	2.5×10^{-14}		240.6	79
$C_3H_7O + HO_2 \rightarrow H_2O_2 + C_3H_6O$	5.0×10^{-13}			*k*
$C_3H_7O + C_3H_7O2 \rightarrow C_3H_7OOH + C_3H_6O$	5.0×10^{-13}			*k*
$C_3H_7O + C_3H_7O \rightarrow C_3H_7OH + C_3H_6O$	3.0×10^{-11}			*k*
$Cl + C_3H_7 \rightarrow HCl + C_3H_6$	7.57×10^{-10}		290	*m*
$Cl + C_3H_7O_2 \rightarrow ClO + C_3H_7O$	7.4×10^{-11}			68[k]
$Cl + HO_2 \rightarrow ClO + OH$	4.1×10^{-11}		450	47
$Cl + HO_2 \rightarrow HCl + O_2$	1.8×10^{-11}		−170	47
$Cl + C_3H_7O \rightarrow C_3H_6O + HCl$	2.0×10^{-11}			69[k]
$CCl_2F + O_2 \rightarrow CCl_2FO_2$	6.16×10^{-30}	−5.61		70
$CCl_2FO_2 \rightarrow CCl_2F + O_2$	3.47×10^{12}	−2.27	11500	*n*
$CCl_2F + Cl \rightarrow CCl_3F$	1.0×10^{-10}			71[o]
$CCl_2F + C_2H_5 \rightarrow HCCl_2F + C_2H_4$	4.7×10^{-11}		−0.5	*k*
$CCl_2F + C_2H_5O_2 \rightarrow C_2H_5O + CCl_2FO$	4.0×10^{-11}			*k*
$CCl_2F + HO_2 \rightarrow OH + CCl_2FO$	1.4×10^{-12}			*p*
$CCl_2F + HO_2 \rightarrow O_2 + CCl_2FH$	$6. \times 10^{-13}$			*k*
$CCl_2F + OH \rightarrow CCl_2FOH$	5.0×10^{-11}			*k*
$CCl_2F + C_3H_7O \rightarrow$ products	2.0×10^{-11}			*k*
$CCl_2F + CCl_2F \rightarrow$ products	1.0×10^{-11}			72[o]

[a] Units of s^{-1} for first-order reactions, cm^3 $molecule^{-1}$ s^{-1} for second-order reactions, and cm^6 $molecule^{-2}$ s^{-1} for third-order reactions. [b] The branching fraction of ref 74 has been fit to the function $\phi = -0.293 + 0.00286\ T - 3.47 \times 10^{-6}\ T^2 + 1.51 \times 10^{-9} T^3$. [c] Rate constant has a pressure dependent term written as 4.5×10^{-32} cm^6 $molecule^{-2}$ s^{-1} [M] + 2.2×10^{-13} cm^3 $molecule^{-1}$ s^{-1} $e^{(599K/T)}$. [d] The temperature dependence of the rate constant is estimated based on that of $C_2H_5O_2 + C_2H_5O_2$.[63] [e] Branching ratio to form C_3H_7O estimated on the basis of the C_2H_5/O_2 system.[63] [f] Estimated on the basis of the mean of the i-$C_3H_7O_2$ and n-$C_3H_7O_2$ self-reaction rate coefficients. [g] Literature value of $C_2H_5O_2 + HO_2$ is used as an estimate of the rate coefficient.[64] [h] Estimated on the basis of $CF_3O_2 + OH$[54]. [i] Estimated on the basis of $C_2H_5OOH + O_2$.[34] [j] Estimated on the basis of i-$C_3H_7 + i$-$C_3H_7O_2$.[78] [k] Estimated on the basis of the CH_3/O_2 system.[52] [l] Estimated on the basis of $C_2H_5O + C_2H_5$.[66] [m] Estimated on the basis of $C_2H_5 + Cl$.[67] [n] Estimated on the basis of the CCl_3F-O_2 bond energy compared to $C_2H_5-O_2$. [o] Estimated on the basis of the CCl_3/O_2 system. [p] Calculated rate constant. [q] The rate constants are written in the form $A(T/298)^n e^{(-E_a/RT)}$.

and the results of the time-dependent master equations was a figure of merit in adjusting the calculated energies of the stationary points in the master equation calculations for propyl + O_2[39] (but not ethyl + O_2). Comparison with HO_2 is therefore partly a test of the accuracy of the parameterization and the correct dependence on total density. Figures 5 and 6 show experimental HO_2 time traces obtained by infrared frequency-modulation spectroscopy, taken from the experiments of refs 17 and 36, at 645 K and total density of 3.25×10^{17} cm^{-3} (the density of the present OH measurements). The previous experiments used Cl_2 as the photolytic source of Cl atoms, so the kinetic model includes reactions of Cl_2 for these cases. As seen in Figures 5 and 6, the parameterized master equation model for both ethyl + O_2 and propyl + O_2 accurately reproduces the

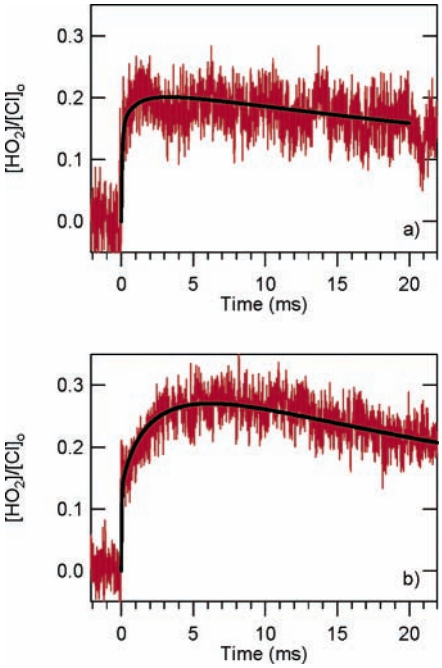

Figure 5. In red are the observed time profiles of HO_2 from the reaction of $C_2H_5 + O_2$ at 645 K and total density of (a) 3.65×10^{17} and (b) 9.0×10^{17} cm^{-3} obtained by infrared frequency modulation spectroscopy.[17] In black are the predicted time profiles of HO_2 from the integrated rate equation model listed in Table 6. Both the formation rate and the total yield of HO_2 observed in the experiment are well reproduced by the model.

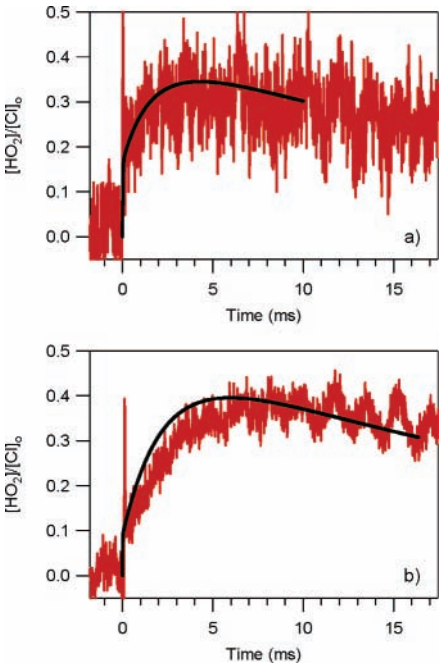

Figure 6. In red are the observed time profiles of HO_2 from the reaction of $C_3H_7 + O_2$ at 645 K and total densities of (a) 3.65×10^{17} and (b) 8.5×10^{17} cm^{-3} obtained by infrared frequency modulation spectroscopy.[36] The black traces are the predicted time profiles of HO_2 from the integrated rate equation model listed in Table 7.

time behavior and amplitude of the HO_2 observed in the previous experiments. The modeled HO_2 production in the propyl + O_2 reaction is slightly faster than observed experimentally, similar to the behavior observed at higher total densities.[39] Given the agreement for the prediction of HO_2 by the model, the next step is to compare predictions of the model for OH formation to the current OH experiments.

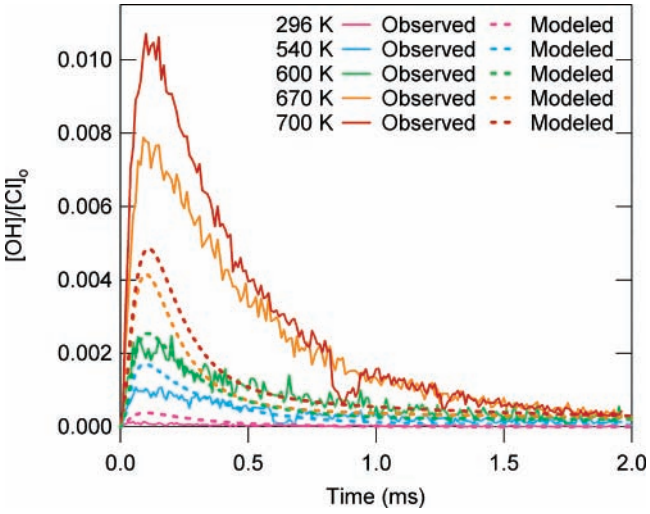

Figure 7. Observed OH time trace for the reaction of $C_2H_5 + O_2$ at the five temperatures measured: 296 (magenta), 530 (cyan), 600 (green), 670 (orange), and 700 K (red). The signal amplitudes have been scaled to $[Cl]_0$ as described in the text. Also shown, as dashed lines, are the OH time traces predicted by the integrated rate equation model in Table 6 at the same five temperatures.

OH Formation. Figure 7 shows observed and predicted OH time traces for ethyl + O_2 at five different temperatures (296, 540, 600, 670, and 700 K), and peak values are given in Table 2. The observed peak $[OH]/[Cl]_0$ dramatically increases between 600 and 700 K. In Figure 4, it can be seen that the time dependent master equations predict that both OH and HO_2 formation should have a biexponential appearance with a fast "prompt" yield and a slower secondary yield. The HO_2 time profiles show this secondary formation at these high temperatures. However, in the OH time traces, this secondary formation is masked by the rapid loss of OH, as is also seen in the integrated rate equation model. The time of the peak [OH] is also reasonably well modeled. Although the model matches the shape of the observed OH trace, it overpredicts the amount of OH formed at low temperatures and underpredicts the amount of OH at higher temperatures.

Figure 8 shows the observed and the predicted OH time traces for propyl + O_2 as a function of temperature, and peak $[OH]/[Cl]_0$ values are given in Table 2. The observed OH time traces for propyl + O_2 are similar in appearance to those of ethyl + O_2, except that the amount of OH formed at each temperature is larger for propyl + O_2. This observation is consistent with both the epoxide yield measurements of Baldwin et al. and the predictions of the time-dependent master equation. The comparison of the model to the observed OH from propyl + O_2 displays a similar discrepancy to that in the ethyl + O_2 system. At lower temperatures the propyl model overpredicts the amount of OH formed, while at higher temperatures the OH is underpredicted. Also, at higher temperatures the model OH peaks at a slightly earlier time than is experimentally observed. Figure 9 compares the model and experimental values for peak $[OH]/[Cl]_0$ as a function of temperature, including estimated uncertainties associated with the experimental data. The discrepancy between model and experiment is small but systematic; the overall increase in the peak $[OH]/[Cl]_0$ with increasing temperature is less pronounced in both the ethyl and propyl + O_2 models than is experimentally observed.

Discussion

The present measurements and the master equation calculations are in agreement that a higher yield of OH is produced in

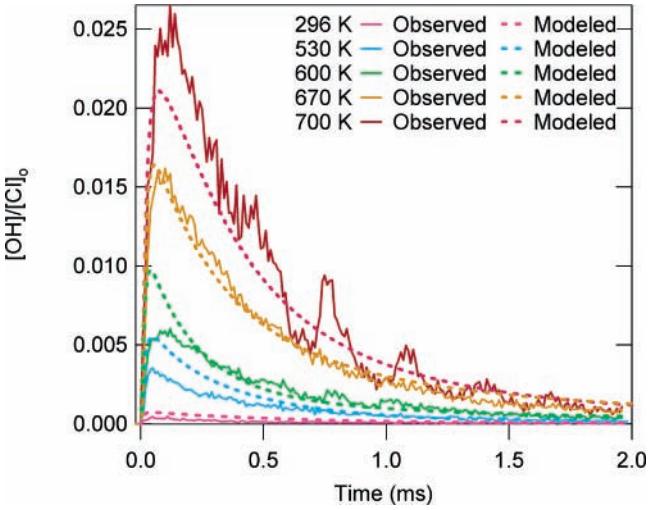

Figure 8. Observed OH time traces for the reaction of $C_3H_7 + O_2$ at the five temperatures measured: 296 (magenta), 530 (cyan), 600 (green), 670 (orange), and 700 K (red). The signal amplitudes have been scaled to $[Cl]_0$ as described in the text. Also shown, as dashed lines, are the OH time traces predicted by the integrated rate equation model in Table 7 at the same five temperatures.

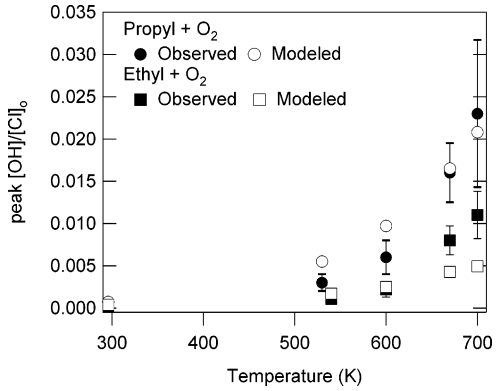

Figure 9. Observed peak $[OH]/[Cl]_0$ from the OH time traces for the reaction of $C_3H_7 + O_2$ (solid circles) and $C_2H_5 + O_2$ (solid squares) at several temperatures. The signal amplitudes have been scaled to $[Cl]_0$ as described in the text. Also shown are the peak $[OH]/[Cl]_0$ from the OH time traces predicted by the integrated rate equation model in Table 6 (open squares) and 7 (open circles) at several temperatures.

the propyl + O_2 reaction than in the ethyl + O_2 reaction. Despite the discrepancy in the apparent activation energy for OH production, the overall yield of OH predicted by the parameterized master equation model is in generally good agreement with the experiment for both ethane and propane oxidation. The ab initio calculations suggest that the dominant $RO_2 \rightarrow$ QOOH isomerization leading to OH formation is similar in these two systems (a 1,4 primary hydrogen shift for the ethyl + O_2 and *i*-propyl + O_2 reactions, and a 1,4 secondary hydrogen shift in the *n*-propyl + O_2 reaction). The difference in the magnitude of OH formation in the two systems is due to the difference in the relative energies of these transition states to isomerization. The master equation calculations predict the difference in yield with reasonable accuracy, raising hopes that these results can be extended to more complicated alkane oxidation systems. Certain aspects of these "prototype" reactions may be directly transferable to larger systems; the 1,4 H transfer in the *n*-butyl + O_2 reaction, which forms OH + 1,2-epoxybutane, has nearly the same barrier to isomerization as the analogous pathway in *n*-propyl + O_2 (forming OH + 1,2-epoxypropane).[39] Nevertheless, some care must be taken to properly account for other competing pathways. There is a calculated low energy barrier for isomerization via a six-membered ring transition state, e.g., the 1,5 primary hydrogen shift in *n*-propyl + O_2 and the 1,5 secondary hydrogen shift in *n*-butyl + O_2.[39] The resulting QOOH isomers have high barriers to either HO_2 or OH formation but may suffer additional reaction with O_2. However, the transition state for the isomerization involving the 1,6 primary hydrogen shift in *n*-butyl + O_2, which has no analogy in the propyl + O_2 reactions, has been calculated to be −9.3 kcal mol^{-1} from the R + O_2 asymptote. This pathway has a relatively low energy pathway to produce tetrahydrofuran + OH. The fact that Baker et al.[8] observe more tetrahydrofuran (1.9%) than 1,2-epoxybutane (1.1%) from addition of *n*-butane to a slowly reacting mixture of $H_2 + O_2$ and N_2 at 753 K suggests that these larger-ring transition states may also play a major role in OH formation in larger alkyl + O_2 reactions. The relative success of the master-equation modeling in the present work suggests that similar calculations may be useful in evaluating larger systems.

A number of possible sources exist for the systematic discrepancy between the experimental and modeled temperature dependence of the OH production, which may have differing consequences for eventual construction of a general model for R + O_2 reactions. Possible deficiencies in the experimental evidence and in the theoretical treatment must be considered, and it must be recognized that comparison of the master equation calculations to experiment relies on assumptions about the kinetics of a number of reactions beyond the R + O_2 system, including several reactions that have not been thoroughly studied.

One interesting question is the importance of QOOH + O_2 in product formation in R + O_2 reactions. The parameterizations of ethyl + O_2 and propyl + O_2 allow the population of these species to be included in the R + O_2 model. Little is known experimentally about the reactions of QOOH species with O_2 despite their postulated importance in chain branching. The model presented here uses the high-pressure limiting rate constants calculated by Bozzelli and Sheng[34] for the $C_2H_4OOH + O_2$ reaction. For the ethane oxidation, this reaction is not very important because at the temperatures of the present experiments very little C_2H_4OOH is formed. Even at 700 K, the equilibrium constant for $C_2H_5O_2$ and C_2H_4OOH still heavily favors $C_2H_5O_2$ and direct formation from R + O_2 is 10^4 slower than formation of $C_2H_5O_2$. Using the rate constant of Bozzelli and Sheng[34] for the addition reaction $C_2H_4OOH + O_2$ and forcing the reaction to directly produce OH still has no discernible effect on the amount of OH formed in the model of Cl-initiated ethane oxidation at 700 K. Applying the same assumption to the propane oxidation model, however, does have a measurable effect on the amount of OH formed (about 18% greater at 700 K). So allowing some direct formation of OH from the QOOH + O_2 reaction would increase the high-temperature yield of OH for Cl-initiated propane oxidation. Given the increased significance of this reaction in larger alkyl radicals, theoretical characterization of larger QOOH + O_2 systems, including master equation calculations of product ratios, appears to be an important area for future work.

One reaction for which there is little experimental evidence, but that is predicted by the model to have an effect on the observed OH formation, is the reaction of R with HO_2. This reaction produces a significant amount of the OH observed at 700 K for the ethane oxidation system. The reaction has relatively less impact for the propane system simply because more OH is produced directly by the $C_3H_7 + O_2$ reaction, while the amount predicted from R + HO_2 is nearly identical in the two systems. The analogous reaction of $CH_3 + HO_2$ has recently been the focus of a theoretical investigation by Zhu and Lin.[53]

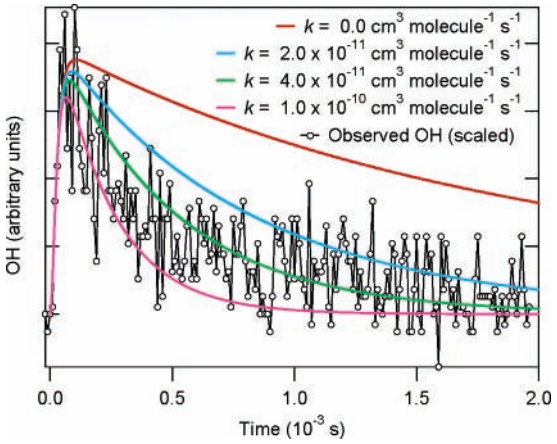

Figure 10. OH time traces predicted by the integrated rate equation model in Table 6 at 296 K by using several different values for the $C_2H_5O_2$ + OH rate constant: 0.0 (red), 2.0×10^{-11} (cyan), 4.0×10^{-11} (green), and 1.0×10^{-10} cm^3 molecule^{-1} s^{-1} (magenta). Also shown as black circles for comparison is the experimentally measured OH time trace (scaled to match the average of the four predicted OH amplitudes).

They calculated that the branching ratio for the products of the reaction should be temperature dependent; however, the dominant product pathway is OH + CH_3O throughout the temperature region of this study. The formation of OH is calculated to be at least an order of magnitude greater than hydrogen abstraction to form O_2 in this temperature region. Also, the reaction is predicted to favor less OH production with increasing temperature, so this reaction may not be a good candidate to dramatically increase OH formation at higher temperature.

The reaction of OH with the alkylperoxy radical, RO_2, is suggested to be an important OH destruction mechanism. This is particularly true at lower temperatures when the major prompt reaction product of R + O_2 is the adduct. Figure 10 shows the predictions of the ethane oxidation model at 296 K with several different values for the rate constant of RO_2 + OH. Although the peak OH concentration is relatively insensitive to the RO_2 + OH reaction, Figure 10 shows that the ethyl + O_2 model does not accurately describe the decay of the OH concentration without including this reaction. Using a value for the $C_2H_5O_2$ + OH rate constant equal to that measured by Biggs et al.[54] for CF_3O_2 + OH does an adequate job of describing the decay of the 296 K OH time trace. Tsang and Hampson[52] estimate the rate constant for the similar reaction CH_3O_2 + OH to be 1×10^{-10} cm^3 molecule^{-1} s^{-1}; using that high a rate constant for $C_2H_5O_2$ appears to overestimate the removal rate of OH in the ethane oxidation system. The present model predicts only a slightly increased sensitivity of the observed OH signal to this reaction at higher radical densities; experiments that permit independent increase of OH and RO_2 concentrations will be necessary to specifically investigate RO_2 + OH reactions. The RO_2 + OH reactions can be important destruction pathways for RO_2 at low temperature and further experimental investigation of their kinetics would seem to be warranted.

Uncertainties in competing reactions, e.g., R + HO_2 and OH + RO_2, may be responsible for some of the discrepancy between the observed OH signal and the master equation model, if the reactions have a significant temperature dependence. However, one should investigate possible changes in the present treatment of the R + O_2 system to improve agreement with experiment, presuming that the estimated rate coefficients for other reactions in the full kinetic model are accurate. It is most instructive to consider the simpler ethyl + O_2 reaction, for which more experimental data is available. The amount of OH formed in the model is largely dependent on the ethyl + O_2 equilibrium and the branching to either C_2H_4O + OH or C_2H_4 + HO_2. These rate constants are based on the solutions to the time-dependent master equation, which previously has been optimized to fit a wide range of experimental results. However, the experimental evidence is not unequivocal; the present OH measurements appear to be closer to Kaiser's[19] recent experimental determination of the oxirane yield (2.5% at 660 K) than to that of Baldwin et al.[12] (~0.8% at 673 K). Lowering the energy barrier to oxirane + OH by 1 kcal mol^{-1} increases the amount of OH produced in the model. Unfortunately, this increases the OH produced at all temperatures, not just high temperature, and does not improve the overall match to experiment. The discrepancy in the observed and predicted temperature dependence in Figure 9 may suggest that the model underestimates the contribution of an OH-producing channel with a significant activation energy. Given the shape of the R + O_2 potential energy surface, channel 1g (or 1j) may appear to be an ideal candidate. Lowering its transition state by 1 kcal mol^{-1} does increase the amount of OH formed at high temperatures; however, such a change cannot be supported by the body of experimental evidence. The experiments of Baldwin et al.[12] and Kaiser[19] appear to agree that the amount of acetaldehyde (channel 1g or 1j) at high temperature is minimal compared to the amount of oxirane (channel 1d or 1i). To match the experiment, the OH formation reactions now in the model should be more dependent on temperature than in the present calculations. To accomplish an increase in apparent activation energy for OH formation while maintaining the present agreement for the overall yield, the A factor for the isomerization must also increase. However, fundamental modification of the calculations to produce detailed agreement with the experiments seems premature in the absence of more reliable independent measurements of rate coefficients of competing reactions such as OH + RO_2 and R + HO_2.

Conclusions

The OH formed from the $Cl/C_2H_6/O_2$ system and the $Cl/C_3H_8/O_2$ system has been measured directly by LIF at several different temperatures. In general, the propyl + O_2 reaction produces more OH at each temperature than the ethyl + O_2 reaction. This observation is consistent with the previous observations of Walker and co-workers[6,12] Baldwin et al. Above 600 K, the peak amplitude of the OH signals from both reactions starts to increase dramatically. The formation of HO_2 from both reactions has previously been predicted by time-dependent master equations. Time-dependent master equations have been used to produce a temperature-dependent parameterization for C_2H_5 + O_2, *i*-C_3H_7 + O_2, and *n*-C_3H_7 + O_2. These parameterizations predict the rate constants for the formation of all of the species involved in the reaction mechanism for R + O_2 (such as R + O_2, RO_2, QOOH, OH + aldehydes, OH + O-heterocycles, HO_2 + alkene). The parameterization is shown to reproduce well the predictions of the time-dependent master equations. These parameterizations are combined with integrated rate equation models for experimental conditions that included both radical formation reactions and radical destruction reactions that occur between the species present in the experiments. Both the HO_2 and OH time traces predicted by that model have been compared to time-resolved experimental measurements. The models accurately describe the formation and amplitude of the HO_2 from both C_2H_5 + O_2 and C_3H_7 + O_2. For both reactions examined, the model underpredicts the amount of OH observed at high temperatures (>600 K) and overpredicts the amount of OH observed at lower temperatures (≤600 K). Important reactions involving OH in the R + O_2 system for which better

experimental data are needed include the reactions of R + HO_2 to form OH and the reaction of RO_2 + OH to remove it.

Acknowledgment. This work is supported by the Division of Chemical Sciences, Geosciences, and Biosciences, the Office of Basic Energy Sciences, the U.S. Department of Energy. Sandia is a multiprogram laboratory operated by Sandia Corporation, a Lockheed Martin Company, for the United States Department of Energy under contract DE-AC04-94-AL85000.

Supporting Information Available: Phenomenological rate coefficients and equilibrium constants for ethyl + O_2 and propyl + O_2 reaction systems as a function of temperature for 30, 760, and 7600 Torr. This material is available free of charge via the Internet at http://pubs.acs.org.

References and Notes

(1) Slagle, I. R.; Ratajczak, E.; Heaven, M. C.; Gutman, D.; Wagner, A. F. *J. Am. Chem. Soc.* **1985**, *107*, 1838.
(2) Knyazev, V. D.; Slagle, I. R. *J. Phys. Chem. A* **1998**, *102*, 1770.
(3) Slagle, I. R.; Park, J.-Y.; Gutman, D. *Proc. Combust. Inst.* **1984**, *20*, 733.
(4) Slagle, I. R.; Ratajczak, E.; Gutman, D. *J. Phys. Chem.* **1986**, *90*, 402.
(5) Slagle, I. R.; Feng, Q.; Gutman, D. *J. Phys. Chem.* **1984**, *88*, 3648.
(6) Baker, R. R.; Baldwin, R. R.; Walker, R. W. *Trans. Faraday Soc.* **1970**, *66*, 3016.
(7) Baldwin, R. R.; Walker, R. W.; Yorke, D. A. *J. Chem. Soc., Faraday Trans. 1* **1973**, *69*, 826.
(8) Baker, R. R.; Baldwin, R. R.; Walker, R. W. *J. Chem. Soc., Faraday Trans. 1* **1975**, *71*, 756.
(9) Baker, R. R.; Baldwin, R. R.; Fuller, A. R.; Walker, R. W. *J. Chem. Soc., Faraday Trans. 1* **1975**, *71*, 736.
(10) Baldwin, R. R.; Cleugh, C. J.; Walker, R. W. *J. Chem. Soc., Faraday Trans. 1* **1976**, *72*, 1715.
(11) Atri, G. M.; Baldwin, R. R.; Evans, G. A.; Walker, R. W. *J. Chem. Soc., Faraday Trans. 1* **1978**, *74*, 366.
(12) Baldwin, R. R.; Pickering, I. A.; Walker, R. W. *J. Chem. Soc., Faraday Trans. 1* **1980**, *76*, 2374.
(13) McAdam, K. G.; Walker, R. W. *J. Chem. Soc., Faraday Trans. 2* **1987**, *83*, 1509.
(14) Gulati, S. K.; Walker, R. W. *J. Chem. Soc., Faraday Trans. 2* **1988**, *84*, 401.
(15) Walker, R. W. Some Burning Problems in Combustion Chemistry. In *Research in Chemical Kinetics*; Compton, R., Hancock, G., Eds.; Elsevier: Amsterdam, 1995; Vol. 3, p 1.
(16) Walker, R. W.; Morley, C. Basic Chemistry of Combustion. In *Low-Temperature Combustion and Autoignition*; Pilling, M. J., Ed.; Elsevier: Amsterdam, 1997; p 1.
(17) Clifford, E. P.; Farrell, J. T.; DeSain, J. D.; Taatjes, C. A. *J. Phys. Chem. A* **2000**, *104*, 11549.
(18) Dobis, O.; Benson, S. W. *J. Am. Chem. Soc.* **1993**, *115*, 8798.
(19) Kaiser, E. W. *J. Phys. Chem. A* **2002**, *106*, 1256.
(20) Kaiser, E. W. *J. Phys. Chem.* **1995**, *99*, 707.
(21) Kaiser, E. W.; Lorkovic, I. M.; Wallington, T. J. *J. Phys. Chem.* **1990**, *94*, 3352.
(22) Kaiser, E. W.; Rimai, L.; Wallington, T. J. *J. Phys. Chem.* **1989**, *93*, 4094.
(23) Kaiser, E. W.; Wallington, T. J.; Andino, J. M. *Chem. Phys. Lett.* **1990**, *168*, 309.
(24) Wagner, A. F.; Slagle, I. R.; Sarzynski, D.; Gutman, D. *J. Phys. Chem.* **1990**, *94*, 1853.
(25) Stark, M. S. *J. Am. Chem. Soc.* **2000**, *122*, 4162.
(26) Rienstra-Kiracofe, J. C.; Allen, W. D.; Schaefer, H. F., III. *J. Phys. Chem A* **2000**, *104*, 9823.
(27) Quelch, G. E.; Gallo, M. M.; Shen, M.; Xie, Y.; Schaefer, H. F., III.; Moncrief, D. *J. Am. Chem. Soc.* **1994**, *116*, 4953.
(28) Quelch, G. E.; Gallo, M. M.; Schaefer, H. F., III. *J. Am. Chem. Soc.* **1992**, *114*, 8239.
(29) Miller, J. A.; Klippenstein, S. J. *Int. J. Chem. Kinet.* **2001**, *33*, 654.
(30) Miller, J. A.; Klippenstein, S. J.; Robertson, S. H. *Proc. Combust. Inst.* **2000**, *28*, 1479.
(31) Ignatyev, I. S.; Xie, Y.; Allen, W. D.; Schaefer, H. F., III. *J. Chem. Phys.* **1997**, *107*, 141.
(32) Chen, C.-J.; Bozzelli, J. W. *J. Phys. Chem. A* **2000**, *104*, 4997.
(33) Bozzelli, J. W.; Dean, A. M. *J. Phys. Chem.* **1990**, *94*, 3313.
(34) Bozzelli, J. W.; Sheng, C. *J. Phys. Chem. A* **2002**, *106*, 1113.
(35) Sheng, C. Y.; Bozzelli, J. W.; Dean, A. M.; Chang, A. Y. *J. Phys. Chem A* **2002**, *106*, 7276.
(36) DeSain, J. D.; Clifford, E. P.; Taatjes, C. A. *J. Phys. Chem. A* **2001**, *105*, 3205.
(37) Kaiser, E. W. *J. Phys. Chem. A* **1998**, *102*, 5903.
(38) Kaiser, E. W.; Wallington, T. J. *J. Phys. Chem.* **1996**, *100*, 18770.
(39) DeSain, J. D.; Taatjes, C. A.; Miller, J. A.; Klippenstein, S. J.; Hahn, D. K. *Faraday Discuss.* **2001**, *119*, 101.
(40) Hughes, K. J.; Halford-Maw, P. A.; Lightfoot, P. D.; Turanyi, T.; Pilling, M. J. *Proc. Combust. Inst.* **1992**, *24*, 645.
(41) Davidson, D. F.; Herbon, J. T.; Horning, D. C.; Hanson, R. K. *Int. J. Chem. Kinet.* **2001**, *33*, 775.
(42) Wagner, A. F.; Slagle, I. R.; Sarzynski, D.; Gutman, D. *J. Phys. Chem.* **1991**, *95*, 1014.
(43) Klippenstein, S. J.; Miller, J. A. *J. Phys. Chem A* **2002**, *106*, 9267.
(44) DeSain, J. D.; Taatjes, C. A. *J. Phys. Chem. A* **2001**, *105*, 6646.
(45) Kohse-Höinghaus, K.; Jeffries, J. B.; Copeland, R. A.; Smith, G. P.; Crosley, D. R. *Proc. Combust. Inst.* **1988**, *22*, 1857.
(46) DeMore, W. B.; Sander, S. P.; Golden, D. M.; Hampson, R. F.; Kurylo, M. J.; Howard, C. J.; Ravishankara, A. R.; Kolb, C. E.; Molina, M. J. *Chemical Kinetics and Photochemical Data for Use in Stratospheric Modeling*; Jet Propulsion Laboratory: Pasadena, CA, 1997.
(47) Atkinson, R.; Baulch, D. L.; Cox, R. A.; Hampson, R. F., Jr.; Kerr, J. A.; Rossi, M. J.; Troe, J. *J. Phys. Chem. Ref. Data* **1997**, *26*, 521.
(48) Lay, T. H.; Bozzelli, J. W. *J. Phys. Chem. A* **1997**, *101*, 9505.
(49) Pitzer, K. S.; Gwinn, W. D. *J. Chem. Phys.* **1942**, *10*, 428.
(50) Knyazev, V. D.; Tsang, W. *J. Phys. Chem. A* **2000**, *104*, 10747.
(51) Klippenstein, S. J.; Wagner, A. F.; Dunbar, R. C.; Wardlaw, D. M.; Robertson, S. H.; Miller, J. A. VARIFLEX; 1.08m ed.; 2001.
(52) Tsang, W.; Hampson, R. F. *J. Phys. Chem. Ref. Data* **1986**, *15*, 1087.
(53) Zhu, R.; Lin, M. C. *J. Phys. Chem. A* **2001**, *105*, 6243.
(54) Biggs, P.; Canosa-Mas, C. E.; Shallcross, D. E.; Vipond, A.; Wayne, R. P. *J. Chem. Soc., Faraday Trans.* **1997**, *93*, 2701.
(55) Grotheer, H.; Riekert, G.; Walter, D.; Just, T. *J. Phys. Chem.* **1988**, *92*, 4028.
(56) Hess, W. P.; Tully, F. P. *J. Phys. Chem.* **1989**, *93*, 1944.
(57) Tsang, W.; Herron, J. T. *J. Phys. Chem. Ref. Data* **1990**, *20*, 609.
(58) Baulch, D. L.; Cobos, C. J.; Cox, R. A.; Esser, C.; Frank, P.; Just, T.; Kerr, J. A.; Pilling, M. J.; Troe, J.; Walker, R. W.; Warnatz, J. *J. Phys. Chem. Ref. Data* **1992**, *21*, 411.
(59) DeSain, J. D.; Jusinski, L. E.; Ho, A. D.; Taatjes, C. A. *Chem. Phys. Lett.* **2001**, *347*, 79.
(60) Pagsberg, P.; Munk, J.; Anastasi, C.; Simpson, V. J. *J. Phys. Chem.* **1989**, *93*, 5162.
(61) Pilgrim, J. S.; McIlroy, A.; Taatjes, C. A. *J. Phys. Chem. A* **1997**, *101*, 1873.
(62) Tully, F. P.; Droege, A. T.; Koszykowski, M. L.; Melius, C. F. *J. Phys. Chem.* **1986**, *90*, 691.
(63) Wallington, T. J.; Dagaut, P.; Kurylo, M. J. *Chem. Rev.* **1992**, *92*, 667.
(64) Maricq, M. M.; Szente, J. J. *J. Phys. Chem.* **1994**, *98*, 2078.
(65) Atkinson, D. B.; Hudgens, J. W. *J. Phys. Chem. A* **1997**, *101*, 3901.
(66) Foucaut, J.-F.; Martin, R. *J. Chim. Phys.* **1978**, *75*, 132.
(67) Maricq, M. M.; Szente, J. J.; Kaiser, E. W. *J. Phys. Chem.* **1993**, *97*, 7970.
(68) Maricq, M. M.; Szente, J. J.; Kaiser, E. W.; Shi, J. *J. Phys. Chem.* **1994**, *98*, 2083.
(69) Daele, V.; Laverdet, G.; Poulet, G. *Int. J. Chem. Kinet.* **1996**, *28*, 589.
(70) Forst, W.; Caralp, F. *J. Chem. Soc., Faraday Trans* **1991**, *87*, 2307.
(71) DeMare, G. R.; Huybrechts, G. *Trans. Faraday Soc.* **1968**, *64*, 1311.
(72) Cobos, C. J.; Troe, J. *J. Chem. Phys.* **1985**, *83*, 1010.
(73) Tschuikow-Roux, E.; Niedzielski, J.; Faraji, F. *Can. J. Chem.* **1985**, *63*, 1093.
(74) Droege, A. T.; Tully, F. P. *J. Phys. Chem.* **1986**, *90*, 1949.
(75) Adachi, H.; Basco, N. *Int. J. Chem. Kinet.* **1982**, *13*, 1125.
(76) Kirsch, L. J.; Parkes, D. A.; Waddington, D. J.; Woolley, A. *J. Chem. Soc., Faraday Trans. 1* **1978**, *74*, 2293.
(77) Tsang, W. *J. Phys. Chem. Ref. Data* **1988**, *17*, 887.
(78) Munk, J.; Pagsberg, P.; Ratajczak, E.; Sillesen, A. *Chem. Phys. Lett.* **1986**, *132*, 417.
(79) Fittschen, C.; Frenzel, A.; Imrik, K.; Devolder, P. *Int. J. Chem. Kinet.* **1999**, *31*, 860.